Testing a model of CO$_2$, water and energy exchange in Great Plains tallgrass prairie and wheat ecosystems

Niall P. Hanan [a,*], Joseph A. Berry [b], Shashi B. Verma [c],
Elizabeth A. Walter-Shea [c], Andrew E. Suyker [c],
George G. Burba [c], A. Scott Denning [d]

[a] *Natural Resource Ecology Laboratory, Colorado State University, Fort Collins, CO 80523, USA*
[b] *Department of Global Ecology, Carnegie Institute of Washington, Stanford, CA 94305, USA*
[c] *School of Natural Resources, University of Nebraska-Lincoln, Lincoln, NE 68583, USA*
[d] *Department of Atmospheric Science, Colorado State University, Fort Collins, CO 80523, USA*

Abstract

A land surface model (a modified version of the Simple Biosphere Model, Version 2; SiB2) was parameterized and tested against two years of eddy covariance flux measurements made over un-grazed tallgrass prairie and a winter wheat field in Oklahoma, USA. The land surface model computed 30-min estimates of sensible and latent heat flux and carbon dioxide flux that agree well with the patterns observed in the field, simulating in particular the contrasting seasonal timing of fluxes in the wheat, where leaf area and physiological activity peak in the spring, and prairie, where leaf area and physiological activity peak in summer. However, systematic errors in flux estimates were also identified for particular times of day and season. These systematic errors are sometimes related to difficulty in correct definition of vegetation structure (LAI) and physiological activity. This was observed particularly in the wheat site towards the end of the growing season when senescence, which reduces both the amount and the physiological activity of leaves, is difficult to parameterize. Simulation errors are also attributed to problems in the mathematical description of water stress, soil respiration, and the leaf-to-canopy scaling methodology. SiB2 tends to predict too much photosynthetic activity at low solar angles, while developing soil moisture stress before it is seen in the field. Systematic errors in energy balance terms (heat and water fluxes) occur for bare soil and dormant vegetation, related to simulation of soil heat flux. Daytime errors in sensible and latent heat fluxes average 20 W m^{-2}, and can be more than 100 W m^{-2} at certain times. In regional and global climate models, the effect of land surface sub-model errors on atmospheric dynamics will depend in part on the magnitude of the systematic error, but also on the spatial extent and temporal duration over which the systematic error persists.

* Corresponding author. Tel.: +1 970 491 0240; fax: +1 970 491 1965.
  E-mail address: niall@nrel.colostate.edu (N.P. Hanan).

1. Introduction

In mid-continental regions the dynamics of the lower atmosphere are closely coupled to the dynamics of the land surface, which provides heat and moisture to the boundary layer and thereby contributes to convective processes, cloud formation and convergence patterns (Yan and Anthes, 1988; Raupach, 1991; Pielke and Vidale, 1995; Wigmosta et al., 1995). Land use changes that alter the timing or magnitude of heating and moistening of the atmosphere can, therefore, affect air temperature, vapor pressure, atmospheric stability and rainfall in the vicinity of the change. The land surface and changes in land use may also impact weather conditions through changes in circulation patterns over much larger regions, extending to continental scales (Charney, 1975; Nobre et al., 1991; Bonan et al., 1992; Polcher and Laval, 1994; Claussen, 1997; Taylor et al., 1997; Stohlgren et al., 1998; Zeng et al., 1999; Wang and Eltahir, 2000; Clark et al., 2001). Mesoscale climate models (operating at grid length scales in the range 10^2–10^5 m) are particularly suited to the study of the effect of land use on regional climate because the land surface can be represented at resolutions appropriate to the landscape. Furthermore, changes in local circulation patterns related to land use can be mechanistically simulated using, in the high resolution case, large eddy simulations to resolve localized flows (e.g. 'lake breeze' effects) caused by adjacent surfaces with differing energy and mass exchange characteristics (Pielke et al., 1992).

Terrestrial vegetation is also a central player in the carbon cycle, from the dynamics of seasonal uptake and release, to long-term source-sink relationships in plant biomass and soil carbon (Moore and Braswell, 1994; Schimel, 1995; Schlesinger and Andrews, 2000; Cramer et al., 2001). Biogeochemical models parameterized at daily or coarser time-steps can successfully simulate seasonal and inter-annual carbon uptake and release (Raich et al., 1991; Parton et al., 1993; VEMAP-Members, 1995), so one could argue that CO_2 uptake and release need not be simulated at the short time-steps (<1 h) required in climate system models for water and heat. Further, short time-scale feedbacks between carbon dioxide exchange and atmospheric dynamics (through radiative heating, for example) are much smaller than the immediate interactions between surface water and energy balance and boundary layer temperature and humidity. On the other hand, the processes that determine CO_2 exchange, particularly photosynthetic uptake, respond directly to high frequency processes (e.g. changes in insolation related to diurnal cycles and cloud passage). Boundary layer humidity, temperature and CO_2 concentration also directly affect photosynthetic and stomatal physiology, and changes in these variables occur at the higher frequency time-scales characteristic of the atmosphere (seconds to minutes). We contend, therefore, that it is desirable to consider the high frequency dynamics of carbon, even if some carbon-related processes, such as plant growth, can be adequately simulated at coarser time-steps. An equally important argument for inclusion of carbon exchange in land surface schemes is that the physiological linkage between photosynthesis and transpiration means that inclusion of 'biology' in land surface models should improve their ability to simulate transpiration and energy partitioning (Randall et al., 1996; Sellers et al., 1996a; Berry et al., 1998), which is still, after all, their primary role. Thus many global and regional atmosphere models now couple water and energy balance with CO_2 exchange, resulting in both better simulation of atmospheric dynamics and contributions to our understanding of the global carbon cycle.

Land use across much of North America has changed dramatically during the last century, with intensification and expansion of agricultural activities in many central and western states contrasting widespread agricultural abandonment and forest re-growth along the eastern seaboard (Turner et al., 1990). In the Great Plains region, agricultural expansion into native grasslands has been extensive, particularly to dryland crops such as wheat and sorghum (Riebsame, 1990). The objective of this study was to test the ability of a land surface model, the simple biosphere model (SiB2; Sellers et al., 1996c), to accurately simulate the fluxes of carbon, water and energy from a native tallgrass prairie and a dryland wheat system. The model used (SiB2) has been incorporated as the land surface scheme in a general circulation model (Randall et al., 1996) and a regional climate model (the mesoscale model RAMS, Denning et al., 2003). Detailed testing of SiB2 in contrasting vegetation types will facilitate assessment of uncertainty when climate system models are

applied in studies of the regional and global impacts of land use options in the Great Plains.

Two contrasting years of eddy covariance flux data (1997, a year with consistent growing season rainfall; and 1998, a year with a long mid-summer drought period; Fig. 1) from two Ameriflux sites were used in this research: a tallgrass prairie site near Shidler, OK, and a rainfed wheat field near Ponca City, OK (Burba and Verma, 2001; Suyker and Verma, 2001). SiB2 was parameterized using local measurements of soil texture, canopy structure and physiology, with more generalized parameter values for some of the less site specific variables. The simulations are compared to measured fluxes to assess model performance and potential sources of error in SiB2.

2. Methods

2.1. The simple biosphere model (SiB2)

The simple biosphere model (SiB2, Sellers et al., 1996c) is a land surface model treating fluxes of water, energy and carbon dioxide from a single-layer canopy. Photosynthesis and net assimilation are computed using equations based on the work of Farquhar, Collatz and colleagues (Farquhar et al., 1980; Collatz et al., 1992), with photosynthesis and stomatal conductance coupled using the Ball-Berry relationship (Ball et al., 1987). We summarize a subset of the equations here related to leaf- and canopy-level photosynthesis (using the notation of Hanan et al.,
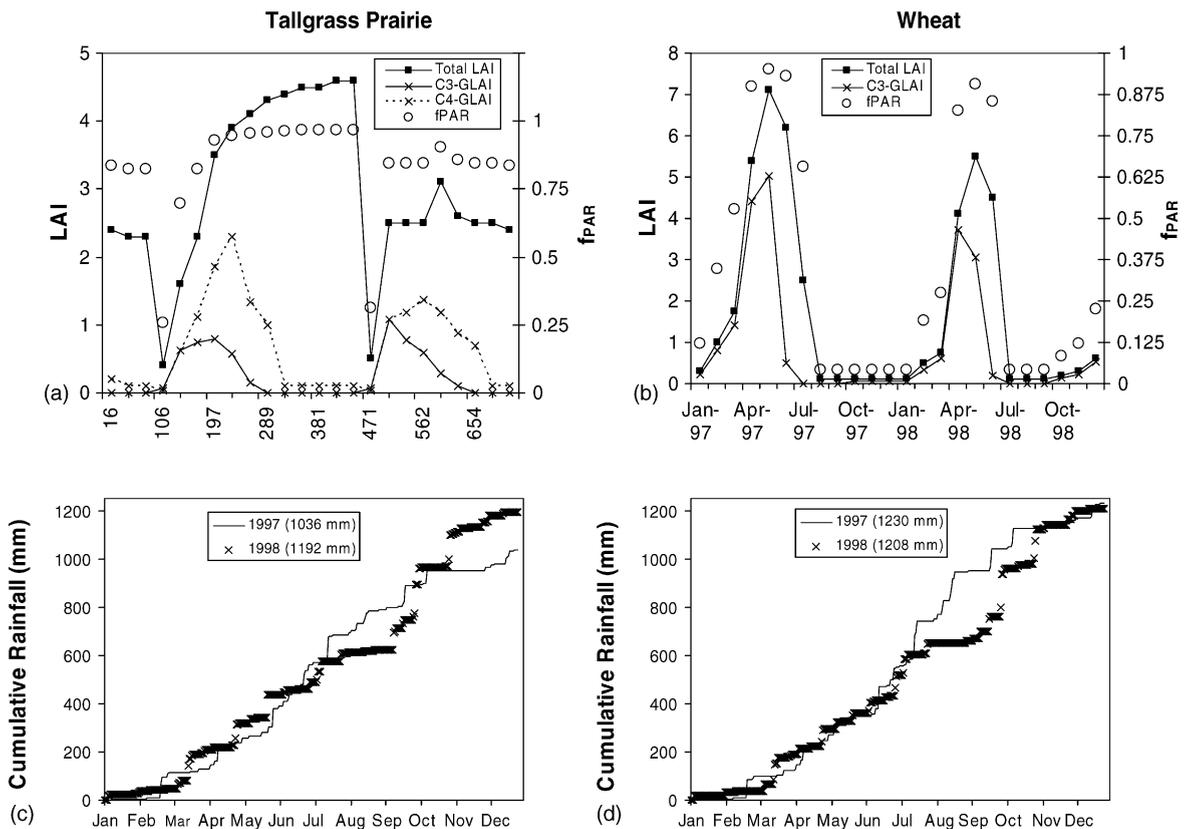

Fig. 1. Field measured canopy structure and rainfall during the simulation period (1997–1998). (a and b) Leaf area and fractional PAR interception (f_{PAR}) for the tallgrass prairie and wheat sites. (c and d) Cumulative rainfall during the 1997–1998 calendar years (with annual totals shown for each site and year in the legends). Leaf area index (LAI) is shown as total (live + dead) and green leaf area (GLAI). Green leaf area at the prairie site is shown for the dominant C_4 species as well as the cool-season C_3 grasses. x-axis scales show day-numbers (starting 1/1/97; for comparison with Figs. 2–4) as well as month and year. A drought period occurred during the summer of 1998 in the period July 30–September 10 (days 576–620) when the prairie was still physiologically active but the wheat site was in fallow.

1998) because they are relevant to later discussion of the leaf-canopy scaling methodology. Leaf-level photosynthesis (A_n) is estimated as the minimum of three processes: the rate of carbon fixation that depends on electron transport and CO_2 availability (j_E; 'light-limited' rate), the rate of carbon fixation defined by Rubisco activity and CO_2 availability (j_C; 'enzyme-limited' rate), and the rate of export of assimilates from the fixation sites (j_S, 'sink-limited' rate). Thus,

$$A_n = [\min] \begin{cases} j_E \\ j_C \\ j_S \end{cases} \quad (1)$$

$$j_E = Q_p \alpha_3 \frac{p_i - \Gamma^*}{p_i + 2\Gamma^*}, \quad \text{for } C_3 \text{ photosynthesis} \quad (2a)$$

$$j_E = \alpha_4 Q_p, \quad \text{for } C_4 \text{ photosynthesis} \quad (2b)$$

$$j_C = V_m \left[\frac{p_i - \Gamma^*}{p_i + K_c(1 + p_{O_2}/K_o)} \right], \quad (3a)$$

for C_3 photosynthesis

$$j_C = V_m, \quad \text{for } C_4 \text{ photosynthesis} \quad (3b)$$

$$j_S = \frac{V_m}{2}, \quad \text{for } C_3 \text{ photosynthesis} \quad (4a)$$

$$j_S = 20{,}000 V_m p_i, \quad \text{for } C_4 \text{ photosynthesis} \quad (4b)$$

where Q_p is the absorbed PAR flux density normal on the leaf surface, p_i the CO_2 partial pressure at the site of carbon fixation, p_{O_2} the partial pressure of oxygen, Γ^* the CO_2 compensation point at ambient O_2 concentration and [min] is evaluated using nested quadratic equations which provide a gradual transition between J (Collatz et al., 1991). The temperature dependencies of the biochemical reactions at leaf temperature (T_l) are described by Q_{10} relationships for the enzyme kinetic parameters (K_c, K_o) and Γ^* and by a Q_{10} relationship with high temperature inhibition for Rubisco activity (V_m), where the reference activities (K_r, V_{mr}), temperature sensitivities and equations are given by Collatz et al. (1991). The intrinsic quantum yield of photosynthetic electron transport (α, mol CO_2 per mol quanta), and the capacity of Rubisco at a reference temperature (V_{mr}, μmol m^{-2} s^{-1}, at 25 °C) are important species-specific parameters of the model.

Sellers et al. (1992, 1996c) developed an elegant solution to the problem of computing the integral photosynthetic flux of a large population of leaves. The method depends on the assumption that leaf nitrogen, and photosynthetic capacity, decline in proportion to average light attenuation through the canopy (Sellers et al., 1992; Kull and Kruijt, 1998). In this idealized situation the leaves of a canopy behave similarly with, for example, light saturation occurring at the same moment in all leaves (though at different light intensities) and internal CO_2 concentration (p_i) being constant. If the decline in solar radiation with depth in a canopy is approximated using Beer's Law, then PAR intensity at a cumulative leaf area l in the canopy is given by $Q_{p,l} = Q_{p,0} e^{-k_\theta l}$ where k_θ is the PAR extinction coefficient for solar radiation from direction θ. Similarly, the canopy profile of photosynthetic capacity is given as $V_{m,l} = V_{m,0} e^{-kl}$. However, in this case, because nitrogen allocation within the canopy is slowly varying, k is averaged over an appropriate time period for that longer term process (e.g. 1 week to 1 month). Thus the full integral expressions for light-limited (J_E) and enzyme-limited (J_C) photosynthesis for C_3 plants are:

$$J_E = \int_0^L Q_{p,0} e^{-k_\theta l} \alpha_3 \frac{p_i - \Gamma^*}{p_i + 2\Gamma^*} \, dl = A_{n,0} \int_0^L e^{-k_\theta l} \, dl$$

$$= A_{n,0} \left[\frac{1 - e^{-k_\theta L}}{k_\theta} \right] = A_{n,0} \frac{f_{PAR\theta}}{k_\theta},$$

for light-limited photosynthesis

$$(5)$$

$$J_C = \int_0^L V_{m,0} e^{-kl} \left[\frac{p_i - \Gamma^*}{p_i + K_c(1 + p_{O_2}/K_o)} \right] dl$$

$$= A_{n,0} \int_0^L e^{-kl} \, dl = A_{n,0} \left[\frac{1 - e^{-kL}}{k} \right] = A_{n,0} \frac{f_{PAR}}{k},$$

for enzyme-limited photosynthesis

$$(6)$$

where J represent the canopy integrals of Eqs. (2) and (3) and similar expressions can be derived for J_S and the corresponding C_4 photosynthesis equations. Thus, given the assumptions of canopy scaling with light availability, the integral canopy flux, whether light-, enzyme- or sink-limited, is given by 'top-leaf' photosynthesis multiplied by a scaling factor ($\Pi = f_{PAR}/k$)

that is approximated by the fraction of incident PAR absorbed by the canopy (f_{PAR}) divided by an extinction coefficient (k). However, the interesting point to note in Eqs. (5) and (6) is the difference in f_{PAR} and k between the light-limited canopy flux, which depends on instantaneous light interception ($f_{PAR\theta}$) and extinction (k_{θ}), and the enzyme-limited canopy flux, which depends on nitrogen allocation and, therefore, on a mean f_{PAR} and k that represent the radiation-weighted PAR availability over several days or longer. In standard SiB2 simulations the factor Π is computed using only the time-mean f_{PAR} (estimated at weekly to monthly time scales, often from satellite measurements, but in this study from field measurements), while k is estimated based on vegetation type (leaf angle distribution and optical properties) and solar geometry for the latitude, longitude and month but does not vary with solar angle. Sellers et al. (1996c) suggest the errors using time-averaged values of k are small: we examine the impacts at low solar angles later in this paper.

Heterotrophic respiration in SiB2 responds to soil moisture and temperature (following Raich and Nadelhoffer, 1989) and is scaled so that annual heterotrophic respiration equals annual net primary production (Denning et al., 1996). Modifications to the basic model are described below. A fuller description of the SiB2 model and associated equation sets can be found in the cited literature.

SiB2 can be parameterized for different vegetation types (grassland, forest and crop lands, broad and needle leaf, deciduous, evergreen, Sellers et al., 1996b). In the standard model the photosynthetic physiology is either C_3 or C_4, but for this study SiB2 was adapted to allow mixed C_3 and C_4 canopies to be simulated. This was achieved by cycling through the photosynthesis subroutines twice, once for each physiological type, calculating separate photosynthetic rates and stomatal conductances, and then estimating a weighted total photosynthetic rate and overall surface conductance from the two components. Total transpiration and canopy energy balance are calculated once for the total canopy with the implicit assumption that the leaves of the two physiological types are well-mixed in the canopy, and that leaf temperatures are similar for the two types.

A modification to the soil water stress functions of SiB2 suggested by Colello et al. (1998) was adopted.

Colello and colleagues found that calculations of canopy water stress using soil water potential scaled between field capacity and wilting point, produced too rapid stomatal closure as the soil dried. This occurred because soil water potential is a highly non-linear function of volumetric water content, making the water stress term highly dependent on the parameters of the volumetric water content to water potential transfer function and very sensitive to small errors in soil water balance. Following the recommendations of Colello et al. (1998) water stress was directly calculated using volumetric water content scaled between field capacity and wilting point. This modification produces a more gradual response of the simulated vegetation canopy to developing soil water deficit.

2.2. Site descriptions

The field study was conducted in a native tallgrass prairie site and a rainfed wheat site in Oklahoma (Burba and Verma, 2001; Suyker and Verma, 2001; Hanan et al., 2002). The tallgrass prairie site (36°56′N, 96°41′W, elevation 350 m above mean sea level) is located 69 km north-east of Ponca City, in north-central Oklahoma and is surrounded for distances of 1–6 km by prairie on gently rolling hills. The micrometeorological instruments were located in a paddock of approximately 500 m × 500 m from which livestock were excluded during the study. A prairie management prescribed burn was conducted in the spring of 1997 and 1998. The vegetation of the prairie site consists of grasses, which occupy over 83% of the site. The most widespread species at the study site are little bluestem [*Schizachyrium scoparium* (Michx.) Nash], sideoats grama [*Bouteloua curtipendula* (Michx.) Torr.], blue grama [*Bouteloua gracilis* (H.B.K.) Lag. *ex* Steud.], and big bluestem (*Andropogon gerardii* Vitman). Forbs comprise about 13% of the vegetation, including annual broomweed (*Amphiachyris dracunculoides* (DC.) Nutt. ex Rydb.), and sedges (*Carex* sp.) occupy approximately 4.3% of the area. Most of the grasses are warm season (C_4) species, which reach peak activity and biomass in the mid-late summer. The C_3 forbs, however, are most active during the cooler spring period. The soil is a silty clay loam of Wolco-Dwight complex (thermic Pachic Argiustolls and mesic Typic Natrustolls) with a 1–2 m layer of dense clay below 0.6 m, and underlying

limestone bedrock. The wheat site (also 500 m × 500 m) is located about 16 km to the north of Ponca City, OK (36°45′N, 97°05′W, elevation 310 m). The relief is flat (0–3°) except for a few small and shallow drainage depressions. The site was planted in winter wheat in mid-fall of each year and was harvested in early summer. Soils are Typic and Pachic Argiustolls of Poncreek and Kirkland complexes, with silt loam and silty clay loam in the upper horizons and heavy clay below 0.6 m. Lower horizons are carbonated due to limestone bedrock.

2.3. Micrometeorological measurements

The micrometeorological and flux measurement systems installed at the two sites in mid-1996 were nearly identical. Fluxes of CO_2, momentum, water and heat were measured at 4.5 m using the eddy covariance technique (e.g. Baldocchi et al., 1988). The eddy covariance sensors included a three dimensional sonic anemometer (Gill Instruments, Lymington, U.K., Model 1012R2) and a closed-path CO_2 analyzer (LI-Cor Inc., Lincoln, Nebraska, Model LI-6262). Details of sensors and data analysis are given in Suyker and Verma (2001). Incoming and outgoing shortwave and net radiation were measured 3.5 m above the soil surface with pyranometers (LI-COR Inc., Model LI-200SA), a four-component solar-thermal radiometer (Kipp & Zonen, Model CNR-1) and a net radiometer (Radiation Energy Balance Systems, Model Q7). Other meteorological variables (air temperature, humidity, mean horizontal wind speed, etc.) were measured at 4.5 m above the soil surface.

2.4. Additional biometric measurements

At both experimental sites, above ground biomass and green and senescent leaf area index (LAI) were estimated by destructive sampling at approximately 2 week intervals (Fig. 1). The harvested vegetation was separated into green, non-green and litter components (described in Suyker et al., 2003). Incoming and outgoing photosynthetically active radiation (PAR) were measured with quantum sensors (LI-COR Inc., Lincoln, NE, Model LI-190SA) located 3 m above the soil surface. Canopy reflected, transmitted, and soil reflected PAR were monitored with light bars (Li-191SA, LiCor Inc., Lincoln, Nebraska), from

which absorbed PAR (APAR) and fractional absorption of PAR (f_{PAR}) were calculated (Burba and Verma, 2001; Hanan et al., 2002). Time domain reflectometer probes (TDR, Environmental Sensors, Victoria, B.C.; Model MP-917) were installed at both sites to measure soil moisture dynamics in profiles to 1 m depth. At the tallgrass prairie site, the fractional contribution of C_3 species to total green-leaf area and PAR interception (P_{C_3}) was assumed to be 0.5 at the start of the growing season, declining monotonically through the season to zero in mid-September. On the wheat site P_{C_3} was set to 1 during the cropping cycle and set to zero between cropping cycles, assuming volunteer growth would be primarily C_4 grasses (Hanan et al., 2002). However, LAI development during the fallow period was very small (<0.05 LAI), thus the C4 component at the wheat site is not shown in Fig. 1. Leaf-level CO_2 and water exchange were measured during the peak growing season at each site using a cuvette gas analyzer (LI-COR Inc., Model Li-6400) to estimate photosynthetic and stomatal physiological parameters used by the SiB2 model.

2.5. Land surface model parameterization

The SiB2 model was parameterized using the field measurements of canopy structure (LAI and fractional PAR interception; Fig. 1), field estimates of maximum Rubisco capacity for photosynthesis (V_{max}), the photosynthesis-stomatal slope function (m, sensu Ball et al., 1987) and soil reflectances (Table 1). All other parameter values were set using biome-specific values and algorithms provided by Sellers et al. (1996b), with soil parameters for a clay to clay-loam soil (tallgrass site) and clay-loam to sandy-clay loam soil (wheat). Meteorological variables measured at each site (temperature, humidity, atmospheric pressure, solar radiation, wind-speed and rainfall) were compiled into continuous data files. For the two years simulated in this study, ground measurements for the six meteorological variables listed above were available for more than 95% of the time at the tallgrass prairie site and more than 90% of the time at the wheat site. Missing values were filled to create a continuous data-set, using interpolation to fill short gaps (<3 h) and measurements from adjacent stations with slope and offset calculated to reduce any systematic error that might occur between stations related to differences in altitude, slope, aspect

Table 1
Physiological and soil reflectance parameters for tallgrass prairie and wheat sites estimated from field measurements

Parameter	Tallgrass site	Wheat site
V_{max}—C_3 (μmol m^{-2} s^{-1})	92.0	150.0
V_{max}—C_4 (μmol m^{-2} s^{-1})	30.0	30.0
m—C_3	10.0	9.0
m—C_4	3.4	4.0
Soil reflectance—visible (%)	10.0	9.9
Soil reflectance—near infrared (%)	17.0	28.9

V_{max} is the maximum Rubisco capacity, defined for plants with C_3 and C_4 photosynthetic pathways (Sellers et al., 1996c). m is the Ball-Berry slope function as used in SiB2 (Ball et al., 1987), also defined for C_3 and C_4 species. All parameters for the model simulations use published values (Sellers et al., 1996b) excepting those presented here and in Fig. 1.

or exposure. The continuous (filled) data were used to 'drive' the model simulations.

The measured fluxes and simulations are compared using two-dimensional plots that show the time of day and day number (starting 1/1/97) on the *x*- and *y*-axes, with the flux magnitude represented in color (Figs. 2–4). In all cases, we follow the micrometeorological convention and represent fluxes towards the land surface as negative values, and fluxes into the atmosphere as positive values. The two-dimensional plots were constructed by calculating 10-day diurnal averages of the half-hourly fluxes centered on the 5th, 15th and 25th day of each month. They thus consist of 48 averages in the *x*-dimension (30-min averages) and 72 averages in the *y*-dimension (10-day averages over two years). The measured and simulated fluxes are also compared in a difference plot (simulated-measured) and a more conventional scatter plot of simulated versus measured fluxes. The value of the difference plots is that they allow the flux measurements and simulations to be compared in their diurnal and seasonal context. In this way, temporally consistent features, and systematic differences between observations and simulations, can be identified and possible causes for systematic errors more easily diagnosed.

3. Results and discussion

3.1. Flux phenology

Differences in the timing and intensity of fluxes represent a primary difference between prairie and wheat sites: the patterns for the three fluxes (CO_2, water and heat) are quite distinct between sites (Figs. 2–4). CO_2 uptake is concentrated during periods of maximal leaf area and physiological activity, which is later in the year for the grassland than for the winter wheat crop (Fig. 2). At the prairie site, C_3 species contribute significantly to the fluxes in the cooler spring months, but the C_4 species surpass the C_3 species in leaf area as the summer progresses (Fig. 1). At the wheat site C_4 volunteers (weeds) make little or no contribution to the fluxes. Latent heat flux is higher for wheat than for prairie in the spring because of earlier LAI development, but soil evaporation makes wheat similar to the prairie in summer, even following wheat harvest in July. The timing of sensible heat flux maxima is inversely correlated with active leaf area (i.e. sensible heat fluxes reduce with increasing green LAI), but is positively correlated with solar season, because of increasing available energy in summer months.

3.2. CO_2 flux

At both sites, the land surface model tends to underestimate nighttime ecosystem respiration during the growing season and overestimate nighttime fluxes when the vegetation is absent or dormant (Fig. 2; see also Fig. 7). In other words, there is more seasonality to ecosystem respiration than currently simulated by the model. Although the errors are relatively small (<3 μmol m^{-2} s^{-1}), the differences are consistent, which could add up to large seasonal and longer-term errors. SiB2 uses a simplified soil respiration scheme based on temperature and soil moisture, with autotrophic respiration based on green leaf area and leaf temperature. The model bias in this regard may be related to a failure to consider the seasonality of soil respiration related to vegetation activity and turnover of labile assimilate in roots and rhizosphere (Hanan et al., 1998; Hogberg et al., 2001; Reichstein et al., 2003).

At the prairie site during the growing season SiB2 overestimates photosynthetic CO_2 uptake in the early morning and late afternoon, particularly during the consistently wet year (1997; Fig. 1). A similar though less pronounced trend is present at the wheat site. We hypothesized that these systematic errors in early morning and late afternoon simulations might arise
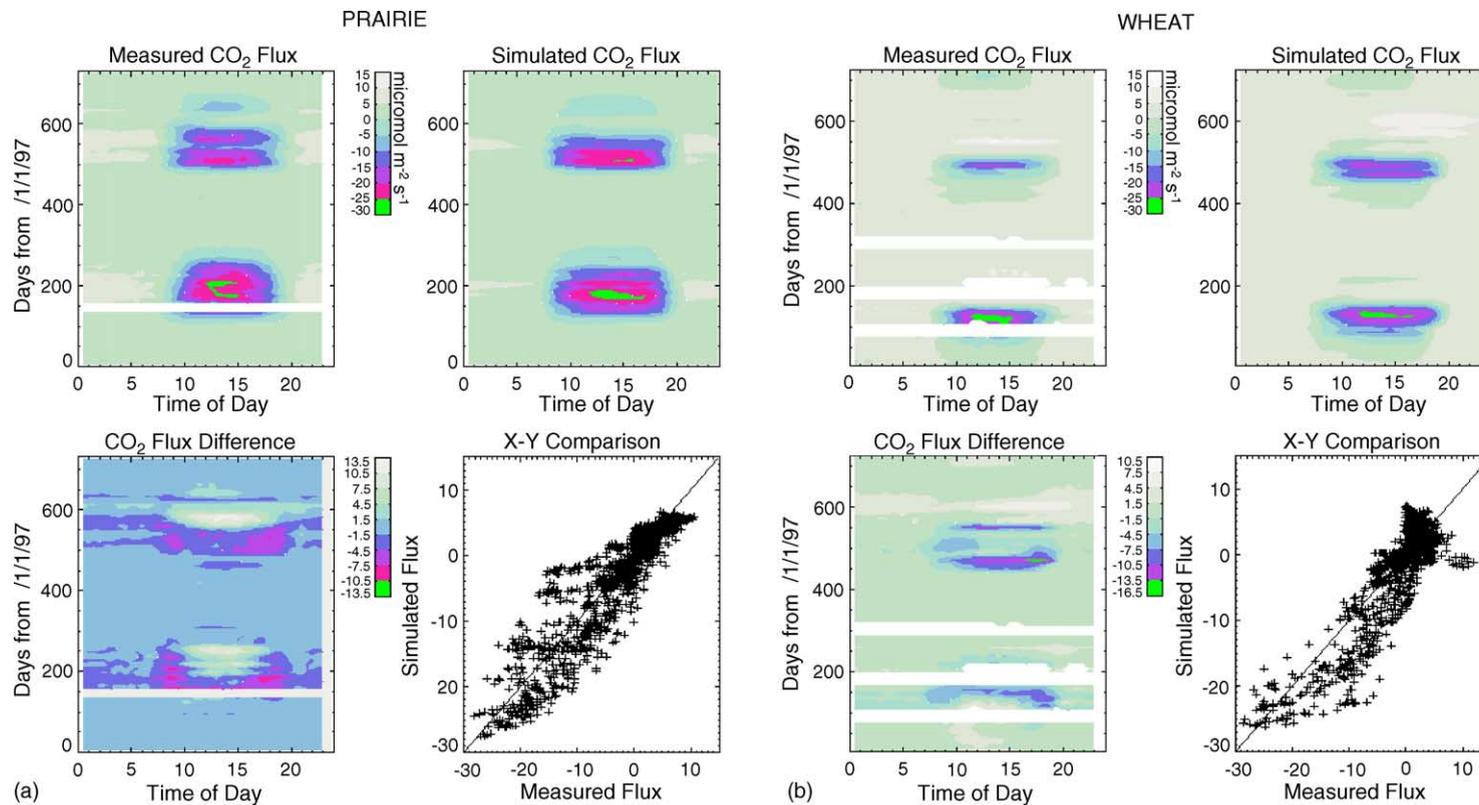
Fig. 2. Daily and inter-annual patterns of measured and simulated CO_2 flux at the tallgrass prairie site (a) and wheat site (b). In all plots, the fluxes are averaged for each 30-min interval over 10 day periods, so that each month of data is represented by three diurnal curves centered on the 5th, 15th and 25th day of the month, resulting in 48 half-hour averages by 72 10-day averages. Surface plot *y*-axis are numbered from 1/1/97 and units are as shown in the upper color-scale. Difference images are calculated as (simulated-measured) such that positive values occur when the model overestimates the measurements. White space in the surface plots indicates no data. The scatter plots show the simulations (averaged as for the surface plots) against measurements, with the 1:1 line shown for comparison.
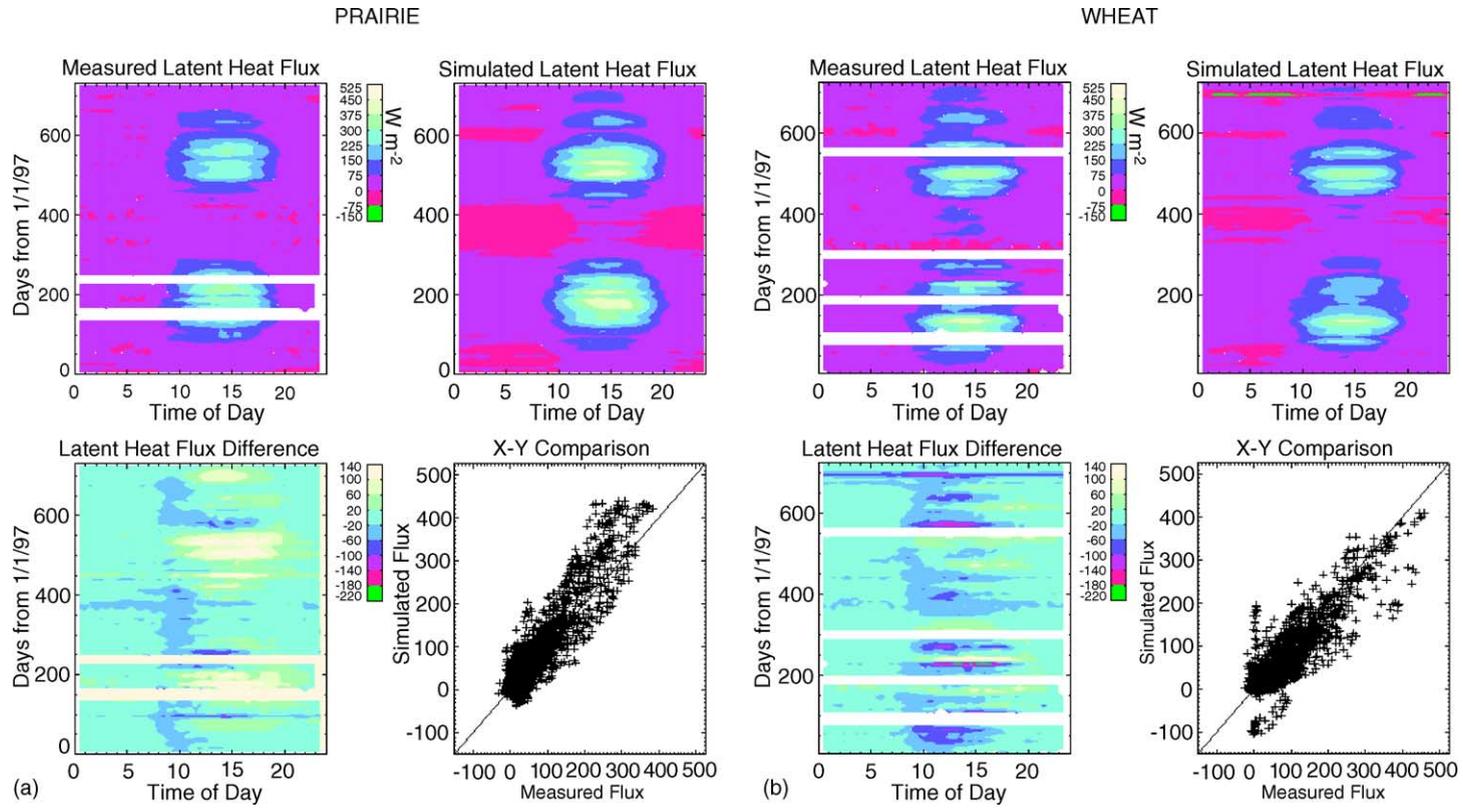
Fig. 3. Daily and inter-annual patterns of measured and simulated latent heat flux at the tallgrass prairie site (a) and wheat site (b); see Fig. 2 legend for other details.
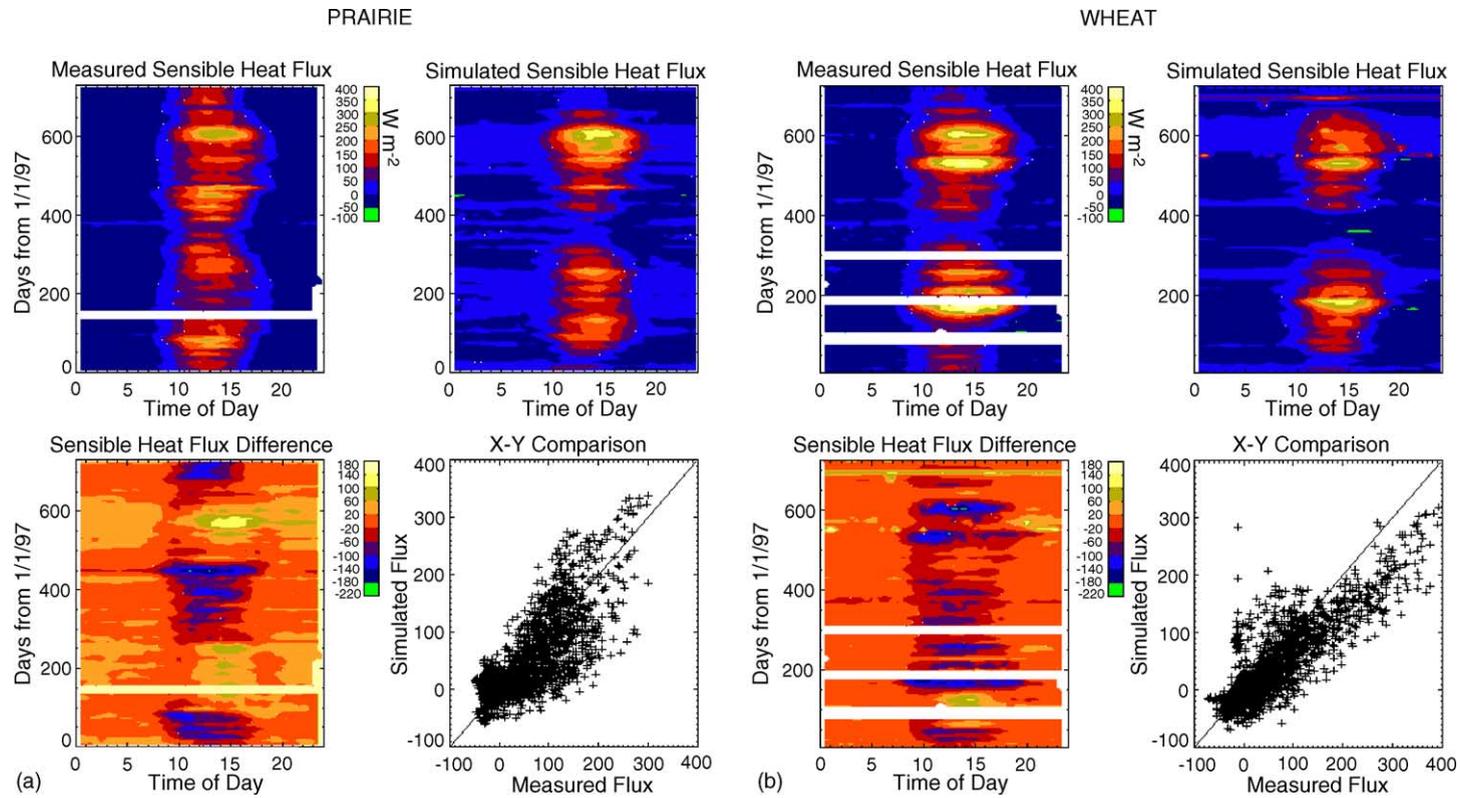
PRAIRIE

WHEAT

Fig. 4. Daily and inter-annual patterns of measured and simulated sensible heat flux at the tallgrass prairie site (a) and wheat site (b); see Fig. 2 legend for other details.

from the use of a constant PAR extinction coefficient (k) and f_{PAR} in light-limited leaf–canopy scaling (Eq. (5)). As discussed earlier, in standard SiB2 implementations k varies with canopy architecture (leaf angle distribution), latitude and day of year in SiB2, but is assumed to be diurnally constant, while f_{PAR} also varies through the year but not diurnally. This scaling is appropriate for light-saturated (enzyme-limited) photosynthesis (Eq. (6)), but may lead to errors in estimation of light-limited photosynthesis. In particular, in the early morning and late afternoon (solar zenith angles $>75°$) the use of a constant k will underestimate actual k_θ by a factor of 2 or more (Fig. 5a). Variability in f_{PAR} with solar angle in near-homogeneous canopies (when LAI $> \sim 2.0$) is much less than variability in k_θ (see, for example, Bégué et al., 1996). However, use of a constant k_θ in the early morning and later afternoon will lead to overestimation of the scaling multiplier (Π) with direct and linear impact on estimated canopy net photosynthesis (Eq. (1)). Although net ecosystem exchange during daylight hours includes both soil respiration and net canopy photosynthesis, model error in assuming constant k_θ when canopy photosynthesis is light-limited will likely manifest also in the net ecosystem exchange estimates.

We examined this hypothesis for clear sky periods using 10-day simulations with diurnally varying estimates of k_θ during mid-June 1997 and 1998 (Fig. 5b and c). Simulations of late afternoon fluxes were improved using variable k_θ. However, the morning simulations during these two periods were similar to simulations using fixed k_θ, in part because the respiratory release of CO_2 (which is different in the two simulations because annual respiration is forced to balance annual NPP) offsets changes in net photosynthesis. During the middle of the day, canopy photosynthesis is presumably light-saturated. Under light-saturated conditions the radiation-weighted mean k (i.e. standard SiB2 simulations) is the appropriate scaling variable (Eq. (6)) and the use of a variable k_θ resulted in overestimation of photosynthetic uptake relative to the measurements and the standard simulations. This serves to emphasize the point that diurnal variability in k_θ is only important when canopy photosynthesis is light limited. Thus operational implementation of a diurnally variable k_θ in the SiB2 model, which
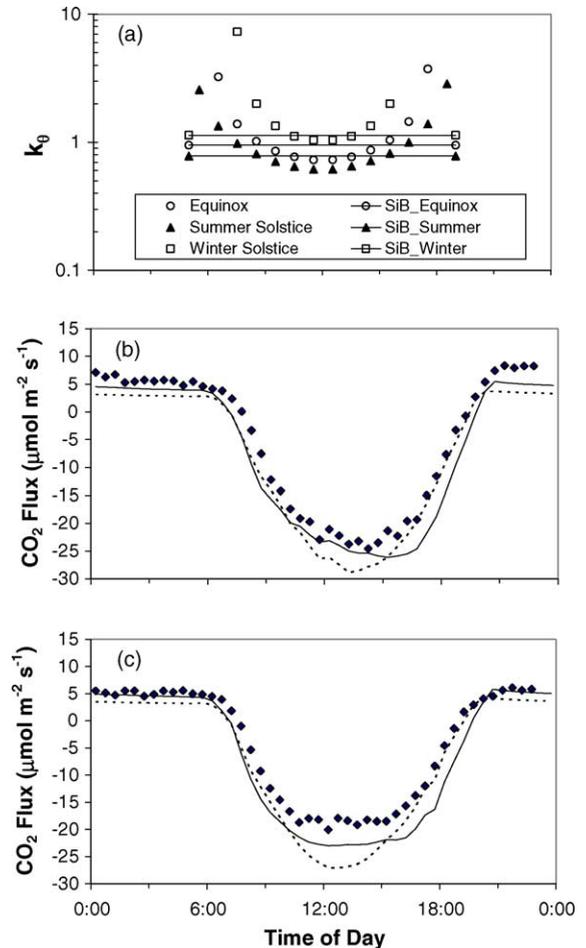

Fig. 5. Impact of diurnally variable k_θ (Eq. (1)) in calculation of net ecosystem CO_2 flux compared to standard SiB2 implementation where k_θ is fixed for each simulation month. (a) k_θ computed for summer and winter solstice and vernal equinox for the latitude of the study sites, for an erectophile canopy (De Wit, 1965; Hanan, 2001) compared to SiB2 fixed values for that location and vegetation type. (b) Ensemble average observations and simulations for a 10-day period near the Summer solstice, June 10–20, 1997 (centered on day 166 in Fig. 2. (c) As above, for June 10–20, 1998 (day 531). Observations (◆) and standard simulations (solid line) are as shown for those time periods in Fig. 2; modified simulations use a diurnally variable k_θ (dotted line).

may provide marginal improvements in the simulations in the early morning or late afternoon, should default back to an appropriate (radiation-weighted) monthly mean k when top leaf photosynthesis switches from light-limitation (Eq. (5)) to enzyme limitation (Eq. (6)).

In this study, we did not fully implement such a scheme for k_θ (i.e. varying at low light but fixed at high light) and we found that the standard SiB2 simulations provide a better estimate of the relatively flat, light saturated, midday CO_2 uptake. Thus while variable k_θ did provide small improvements to simulations at low sun angle, subsequent analyses in this paper utilize the standard simulations as shown in Figs. 2–4.

SiB2 predicts up to 10 μmol m^{-2} s^{-1} too little photosynthetic uptake during the middle of the day at the prairie site in mid- to late growing season, particularly during the drought period of 1998 (days 550–600 in Fig. 2a). It appears that, even with the Colello et al. (1998) modifications to the water stress subroutine, the model still develops too much water stress in response to drying soils, leading to an unrealistic reduction in simulated photosynthetic activity of the prairie canopy. At the wheat site, growth is concentrated in the cooler and wetter months before July (and the crop was harvested before the August 1998 drought) so this water stress phenomenon was not observed. On the contrary, at the wheat site, SiB2 predicts up to 10 μmol m^{-2} s^{-1} excess photosynthetic uptake towards the end of the growing season, particularly in 1997 (circa day 150). In this case, the physiological activity of "green" leaf area may have been overestimated: during maturation and grain filling stages, the lower leaves of the wheat plant begin to senesce and the photosynthetic capacity of apparently green leaves declines (Pearman et al., 1979). Physiological changes of this sort are hard to determine without frequent measurements during the growing season and were not taken into account in the physiological parameterization of the model.

The scatter plots of observations versus simulations (Fig. 2) show the overall performance of the carbon flux component of SiB2 during the two-year period. For the two sites, although maximum observed errors are of similar magnitude (up to 12 μmol m^{-2} s^{-1}) there is more systematic error in model estimates at the wheat site, probably caused by the overestimation of photosynthetic uptake during mid- and late growing season discussed above. The scatter plots are useful to show overall performance, model consistency and systematic error. However, they do not immediately indicate when and where SiB2 is failing to represent the measured fluxes: combination with the adjacent two-dimensional difference plots allows better interpretation of the source and likely cause of errors.

3.3. Latent heat flux

SiB2 overestimates the frequency of nighttime dewfall, and underestimates early morning latent heat fluxes (LE) at both sites during the winter months (cf. negative nighttime fluxes and relatively small morning fluxes in the simulations of Fig. 3). When the vegetation is dormant, CO_2 and latent heat fluxes are less closely coupled than during active growth, both in reality and in model simulations. Underestimation of early morning LE (8:00–10:00 a.m. in Fig. 3) indicates that the model may underestimate the importance of evaporation from soil and dew, especially during winter mornings. At the wheat site, there is also modest underestimation of latent heat flux in winter. During the early summer at the prairie site the model overestimate midday and afternoon latent heat flux by up to 100 W m^{-2}. However, during the drought period of the second year (days 576–620) latent heat flux at both sites is underestimated. The model may thus underestimate the impact of higher temperatures and vapor pressure deficit on stomatal closure in wet conditions (Farquhar and Sharkey, 1982), while overestimating drought stress in dry conditions.

The postulated influence of low solar angle, and consequent error in the scalar multiplier Π, on estimation of CO_2 flux does not translate to consistent overestimation of canopy latent heat flux in the morning or afternoon periods. Indeed, simulated latent heat fluxes were very similar for the mid-June 1997 and 1998 periods when using both fixed and variable k_θ (data not shown). This may occur because Π is not used directly in calculation of canopy transpiration, but is used to estimate surface conductance. Transpiration is calculated as the product of the leaf-atmosphere vapor pressure gradient and the surface conductance and thus LE remains very dependant on atmospheric demand (i.e. vapor pressure deficit).

The plots of simulated and measured fluxes in Fig. 3 indicate generally good performance of SiB2, but with confirmation that during peak latent heat flux periods the model tends to overestimate prairie LE and slightly underestimate wheat LE.

3.4. Sensible heat flux

At the prairie site growing season nighttime inversions (negative sensible heat flux) are common

in the observations but relatively rare in the simulations (Fig. 4). Furthermore at the prairie site, the model tends to overestimate daytime sensible heat flux (by ~100 W m^{-2}) during the growing season and underestimate it (by ~100 W m^{-2}) during the dormant periods. At the wheat site, the model also underestimates dormant season daytime sensible heat flux, even though the dormant period for wheat occurs at a different time of year than in the prairie system (including most of the summer months after harvest and prior to September planting). The consistency between sites in sign and magnitude of these relatively large (~100 W m^{-2}) dormant season daytime sensible heat flux errors indicated that the model may underestimate net radiation or available energy in the absence of a physiologically active canopy. To explore this hypothesis we examined the net radiation and available energy balance terms computed by the SiB2 model for the months June and December 1997 at the prairie site and compared these estimates with field observations (Fig. 6). This represents an independent test of the radiation balance components of SiB2 which uses measurements of incoming shortwave and longwave radiation as input and then computes net radiation at the soil-vegetation surface (R_n), flux of energy into the soil column (G) and available energy (R_n–G). The data in Fig. 6a and b suggest that shortwave radiative transfer, surface albedo and longwave emission components of R_n are well simulated by the model in both months. However, simulations of the available energy term (R_n–G) are similar to measurements during the growing season (Fig. 6c) but are much less than observed in the dormant season (Fig. 6d). This occurs because soil heat flux (G) in the model predicts much higher G than observed in December (Fig. 6f), which results in underestimation of the available energy. The daytime errors are offset on a >24 h time-scale by negative soil heat flux and small overestimates of available energy at night such that energy conservation in the soil is maintained. The dormant season error in estimates of daytime R_n–G is of similar magnitude to the systematic error in sensible heat flux, suggesting that the sensible heat flux errors result from, and compensate, errors in simulation of soil heat flux and available energy. Comparison of the energy balance terms for the months of June and December 1997 indicate that G, and consequently (R_n–G), are

much more accurately simulated under a developed and physiologically active canopy than in the physiologically inactive and low LAI of the winter-time canopy.

At the prairie site the scatter plot of simulated and measured sensible heat flux (Fig. 4) indicates no systematic error, but considerable spread around the 1:1 line, whereas at the wheat site, the underestimation of dormant season (i.e. late summer when heat fluxes are relatively high) sensible heat flux produces a consistent deviation below the 1:1 line.

3.5. Seasonal and diurnal model performance

Model performance is assessed for different seasons and times of day in Fig. 7. In these plots the average error (simulated-measured) is shown to highlight any systematic error, with the 90th and 10th percentiles as an indication of the distribution of errors observed within each defined time period.

Daytime CO_2 fluxes at the prairie site show little or no systematic error, but considerable error range, in part because average fluxes are large. At night, the model underestimates respiratory loss in the growing season and overestimates in the dormant season (as seen in Fig. 2). However, the nighttime error range is smaller than during daylight because the fluxes are generally small. The results for the wheat site are similar, except that CO_2 uptake (negative values) is overestimated during the growing season, related to the end of season overestimation of photosynthetic capacity discussed above. Latent and sensible heat fluxes are consistently overestimated at the prairie site during the growing season, by a total (LE+H) of approximately 40 W m^{-2}, when averaged from 6:00 a.m. to 6:00 p.m. At the wheat site this trend is less evident because the LE overestimate in 1997 growing season is balanced by an underestimate in the drier 1998 cropping season (Fig. 7 shows averages for 1997 and 1998). In the dormant months the average error in estimating latent heat flux is relatively low for both sites, but the daytime sensible heat flux is consistently underestimated, reflecting the under-estimation of available energy shown in Fig. 6.

The 10th and 90th percentiles in Fig. 7 indicate that deviations during individual 30-min periods can be much higher than the averages. Such errors, particu-larly in the sensible and latent heat terms, may be
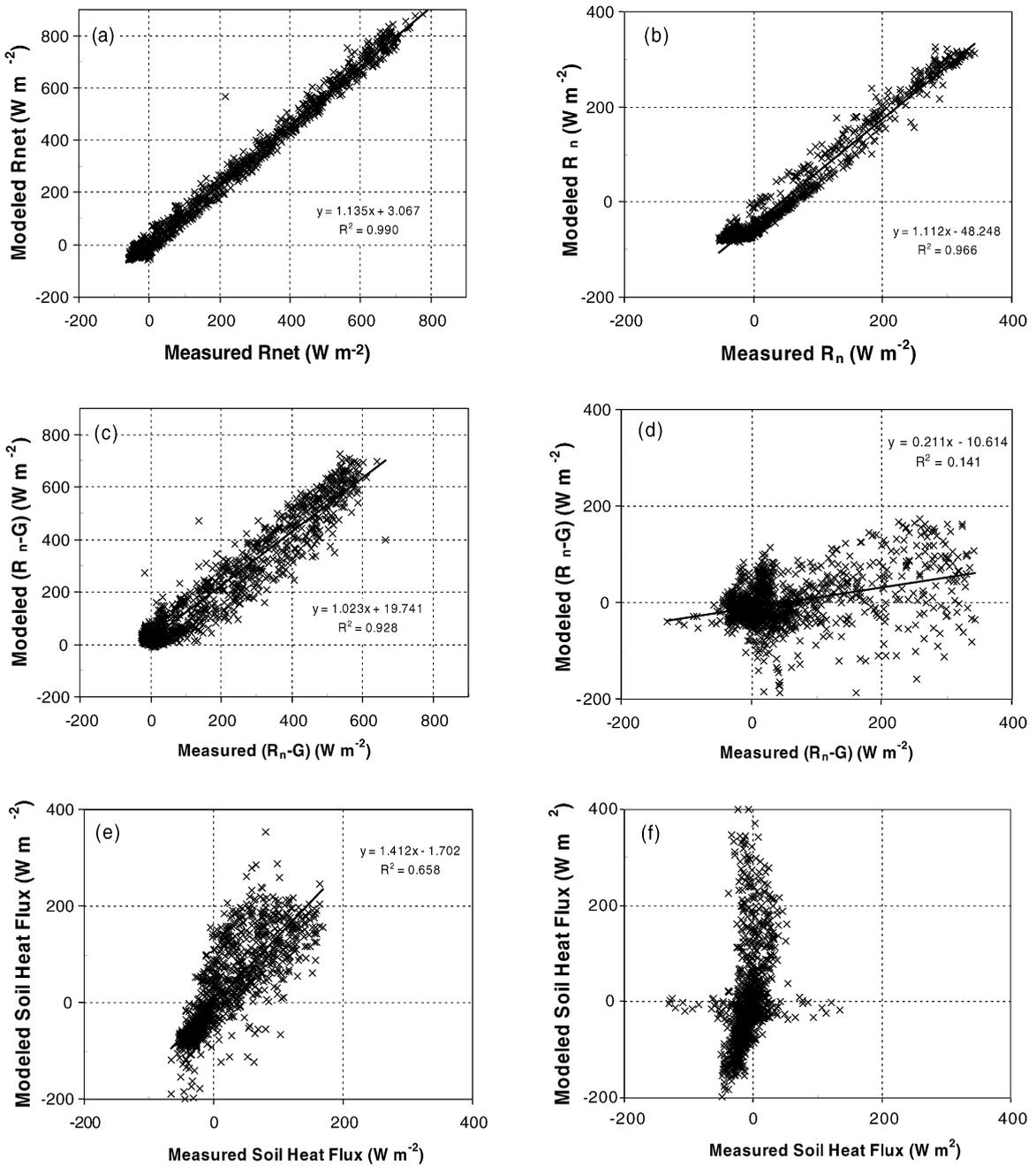
Fig. 6. Summer and winter energy balance calculations for the prairie site (June 1997 in left column, December 1997 in right column; 30 min averages). Panels show (a and b) observed and simulated net radiation (R_n), (c and d) available energy (R_n–G) and (e and f) soil heat flux (G). Data in these plots correspond to days 152–181 (June) 335–365 (December) in Fig. 4a.
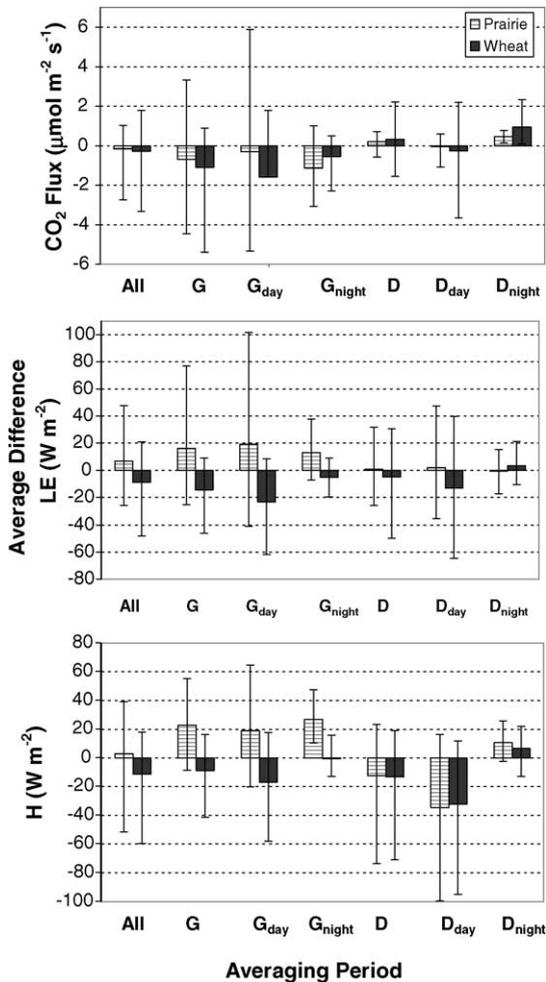
Fig. 7. Land surface model performance indicated by the average difference between measured and simulated fluxes during different time periods at the tallgrass prairie and wheat sites. Positive values occur when the model overestimates the measurements. Averaging periods are defined for: the full two-year data sets (all), the growing season (G), daytime and nighttime hours of the growing season (G_d and G_n), the "dormant" season (D), and daytime and nighttime hours of the dormant season (D_d and D_n). The error bars show the 10th and 90th percentile of observed deviations (i.e. 80% of contrasts between observations and simulations fall within the error ranges shown). Growing seasons are defined by the period of net daytime uptake (Suyker and Verma, 2001, 2003) which, for the tallgrass prairie site, were 4/27/97–9/30/97 and 4/30/98–10/22/98, with the remainder of the year defined as the dormant season. The growing seasons for winter wheat crop were 1/1/97–5/31/97 and 1/1/98–5/28/98. "Daytime" is defined as 6:00 a.m. to 6:00 p.m. (local time) for the calculations in this figure. Average errors were computed for the 10-day ensembles shown in Figs. 2–4.

cause for concern in coupled (land surface–atmosphere) simulations because of direct impacts on atmospheric dynamics and weather simulations. For example, an error of $100 \, \text{W m}^{-2}$ in estimation of sensible heat flux, particularly if the error occurred consistently in a large region of the atmosphere model domain, would tend to alter pressure and temperature gradients that could result in false predictions of winds and convergence patterns. On the other hand, the energy balance components (heat and water fluxes) of SiB2 (and other land surface models) are somewhat "resistant" to long-term drift because of negative feedbacks in the system. For example, an error in sensible heat flux prediction in one time step will lead to an incremental change in surface temperatures in the following time step that will tend to redress the balance. Similarly, errors in evapotranspiration estimates lead to slight changes in soil and vegetation moisture conditions that constrain the system in following time steps. Furthermore for long-term water balance simulations, the soil-vegetation system is physically constrained between a saturated soil and a very dry soil. Given such physical constraints, long-term drought and heavy rainfall in effect "reset" the water balance components of the model (i.e. both model and reality are forced towards the physical limits), thus redressing, temporarily at least, any long-term bias in simulations that may occur during more mesic periods of the simulation.

4. Conclusions

The two-dimensional plots (Figs. 2–4) provide a way to visualize and interpret long-term flux observations and model simulations. In particular, the difference plot can be used to assess model performance and assist in identification of times of day, and times of year, when the model is less able to predict the measured flux patterns. The visual identification of coherent deviations between measurements and model aids in formulation of hypotheses explaining model errors. Identifying and explaining periods of poor model performance can be difficult when results are not presented in a way that highlights these diurnal and seasonal contexts. The scatter plots of measured versus simulated fluxes (Figs. 2–4) are useful for assessing overall model

performance, but do not provide much information on the timing or reason for model discrepancies.

While model performance is generally good (Fig. 7), the analyses indicate areas where biological or physical processes may not be adequately handled, or where model parameterization does not fully represent the biophysical and physiological status of the ecosystem. For example, the problems encountered in simulating the seasonal patterns of ecosystem respiration might be solved by incorporation of a more detailed biogeochemical sub-model to simulate the allocation of photosynthate, root and shoot growth and evolution of CO_2 from soil carbon pools. Similarly, bias in dormant season soil heat flux appears to result in systematic errors in sensible heat flux (Fig. 6). These errors might be reduced through implementation of improved soil physics components which are currently being implemented for newer versions of the model. Conversely, though we anticipated that using variable k_θ (Eq. (5)) would provide improved simulations of the diurnal cycle of CO_2 flux, test simulations for mid-growing season at the prairie site were not consistently better than using a fixed k_θ. This unexpected result suggests the need for further exploration, including possible re-evaluation of the generality of the scaling paradigm represented in Eqs. (5) and (6) for situations where physiological capacity may not scale with light intensity through the canopy (Evans, 1993; Anten et al., 1995; Meir et al., 2002).

Differences in flux magnitude between vegetation types and, in particular, differences in ''flux phenology'', suggest that large-scale land-use change can have, perhaps already has had, broad impact on regional atmospheric boundary layer dynamics and weather. For example, Stohlgren et al. (1998) used a coupled land surface–atmosphere model to demonstrate how transformation to agriculture along the Colorado Front Range could alter convective activity in the region and thus impact regional precipitation. In this study, reductions in sensible heat flux over winter wheat in Oklahoma, compared to prairie, might reduce convective cloud formation in late spring and early summer, and thus potentially delay the onset of summer rains or reduce annual precipitation totals.

In human-dominated landscapes which now predominate in many parts of the world (Matthew, 1983), land use change associated with demographic and economic drivers can produce relatively long-term changes, such as conversion to agriculture or agricultural abandonment, or short term changes in crop selection and management practices. Coupled land surface–atmosphere models are an important tool for exploration of the interactions and feedbacks between surface biology, biophysics and atmospheric dynamics. In particular, coupled models facilitate exploration of the direct impacts that land use decisions at local to national scales may have on regional weather patterns (Pielke et al., 1998). However, the impact of errors in land surface model predictions of surface energy partitioning on regional and global climate model simulations is poorly known. In this study for example, SiB2 consistently overestimated sensible plus latent heat flux during growing season daytimes in the prairie (by on average 40 W m^{-2}), while underestimating sensible plus latent heat flux from wheat by a similar amount. What magnitude of error, over what spatial area, is acceptable for climate model simulations of atmospheric processes? The answer to this question is complex, depending not only on the magnitude and spatial-temporal persistence of systematic errors, but also on the state of the atmosphere and the degree of contrast with adjacent earth surfaces, that modify how the atmosphere will respond to such a systematic error. Given changing land use and human management of terrestrial systems around the world, future efforts to reduce land surface model errors, and understand the significance of errors, in climate system models are of great importance to our understanding of atmospheric dynamics and terrestrial biogeochemical cycles and the impact of human societies in the coupled biosphere–atmosphere system.

References

Anten, N.P.R., Schieving, F., Werger, M.J.A., 1995. Patterns of light and nitrogen distribution in relation to whole canopy carbon gain in C3 and C4 mono- and di-cotyledonous species. Oecologia 101, 504–513.

Baldocchi, D.D., Hicks, B.B., Meyers, T.P., 1988. Measuring biosphere–atmosphere exchanges of biologically related gases with micrometeorological techniques. Ecology 69, 1331–1340.

Ball, J.T., Woodrow, I.E., Berry, J.A., 1987. A model predicting stomatal conductance and its contribution to the control of photosynthesis under different environmental conditions. In: Biggens, J. (Ed.), Progress in Photosynthesis Research. Martinus Nijhoff, Dordrecht, pp. 221–224.

Bégué, A., Roujean, J.L., Hanan, N.P., Prince, S.D., Thawley, M., Huete, A., Tanré, D., 1996. Shortwave radiation budget of Sahelian vegetation. 1. Techniques of measurement and results during HAPEX-Sahel. Agric. Forest Meteorol. 79, 79–96.

Berry, J.A., Raupach, M.R., Hanan, N.P., 1998. Improving SVAT processes in GCMs: vegetation structure, dynamics and physiology. In: A.J., Dolman, R.E., Dickinson (Eds.), Land Surface Parameterizations/Soil Vegetation-Atmosphere Transfer, Schemes, Conclusions. Working Group Reports of a Workshop, La Jolla, CA, 10–14 February, 1997. GEWEX-WCRP, Report No. 31, Washington DC.

Bonan, G., Pollard, D., Thompson, S., 1992. Effects of boreal vegetation on global climate. Nature 359, 716–718.

Burba, G.G., Verma, S.B., 2001. Prairie growth, PAR albedo and seasonal distribution of energy. Agric. Forest Meteorol. 107, 227–240.

Charney, J., 1975. Dynamics of deserts and drought in the Sahel. Quart. J. R. Meteorol. Soc. 101, 193–202.

Clark, D., Xue, Y., Harding, R., Valdes, P., 2001. Modeling the impact of land surface degradation on the climate of tropical north Africa. J. Climate 14, 1809–1822.

Claussen, M., 1997. Modeling bio-geophysical feedback in the African and Indian monsoon region. Climate Dyn. 13, 247–257.

Colello, G.D., Grivet, C., Sellers, P.J., Berry, J.A., 1998. Modeling of energy, water and CO_2 flux in a temperate grassland ecosystem with SiB2: May–October 1987. J. Atmos. Sci. 55, 1141–1169.

Collatz, G.J., Ball, J.T., Grivet, C., Berry, J.A., 1991. Physiological and environmental regulation of stomatal conductance, photosynthesis and transpiration: a model that includes a laminar boundary layer. Agric. Forest Meteorol. 54, 107–136.

Collatz, G.J., Ribas-Carbo, M., Ball, J.A., 1992. Coupled photosynthesis-stomatal conductance model for leaves of C4 plants. Aust. J. Plant Physiol. 19, 519–538.

Cramer, W., Bondeau, A., Woodward, F.I., Prentice, I.C., Betts, R.A., Brovkin, V., Cox, P.M., Fisher, V., Foley, J.A., Friend, A.D., Kucharik, C., Lomas, M.R., Ramankutty, N., Sitch, S., Smith, B., White, A., Young-Molling, C., 2001. Global response of terrestrial ecosystem structure and function to CO_2 and climate change: results from six dynamic global vegetation models. Global Change Biol. 7, 357–373.

De Wit, C.T., 1965. Photosynthesis of Leaf Canopies, vol. 663. Centre for Agricultural Publishing and Documentation (Pudoc), Wageningen, The Netherlands.

Denning, A.S., Collatz, G.J., Zhang, C.G., Randall, D.A., Berry, J.A., Sellers, P.J., Colello, G.D., Dazlich, D.A., 1996. Simulations of terrestrial carbon metabolism and atmospheric CO_2 in a general circulation model. 1. Surface carbon fluxes. Tellus Series B. Chem. Phys. Meteorol. 48, 521–542.

Denning, A.S., Nicholls, M., Prihodko, L., Baker, I., Vidale, P.-L., Davis, K.J., Bakwin, P.S., 2003. Simulated variations in atmospheric CO_2 over a Wisconsin forest using a coupled ecosystem-atmosphere model. Global Change Biol. 9, 1241–1250.

Evans, J.R., 1993. Photosynthetic acclimation and nitrogen partitioning within a lucerne canopy. II. Stability through time and comparison with a theoretical optimum. Aust. J. Plant Physiol. 20, 69–82.

Farquhar, G.D., Sharkey, T.D., 1982. Stomatal conductance and photosynthesis. Annu. Rev. Plant Physiol. 33, 317–345.

Farquhar, G.D., von Caemmerer, S., Berry, J.A., 1980. A biochemical model of photosynthetic CO_2 assimilation in leaves of C3 species. Planta 149, 78–90.

Hanan, N.P., 2001. Enhanced two-layer radiative transfer scheme for a land surface model with a discontinuous upper canopy. Agric. Forest Meteorol. 109, 265–281.

Hanan, N.P., Burba, G., Verma, S.B., Berry, J.A., Suyker, A., Walter-Shea, E.A., 2002. Inversion of net ecosystem CO_2 flux measurements for estimation of canopy PAR absorption. Global Change Biol. 8, 563–574.

Hanan, N.P., Kabat, P., Dolman, A.J., Elbers, J.A., 1998. Photosynthesis and carbon balance of a Sahelian fallow savanna. Global Change Biol. 4, 523–538.

Hogberg, P., Nordgren, A., Buchmann, N., Taylor, A., Ekblad, A., Hogberg, M., Nyberg, G., Ottosson-Lofvenius, M., Read, D., 2001. Large-scale forest girdling shows that current photosynthesis drives soil respiration. Nature 411, 789–792.

Kull, O., Kruijt, B., 1998. Leaf photosynthetic light response: a mechanistic model for scaling photosynthesis to leaves and canopies. Funct. Ecol. 12, 767–777.

Matthew, E., 1983. Global vegetation and land use: new high-resolution data bases for climate studies. J. Climate Appl. Meteorol. 22, 474–487.

Meir, P., Kruijt, B., Broadmeadow, M., Barbosa, E., Kull, O., Carswell, F., Nobre, A., Jarvis, P.G., 2002. Acclimation of photosynthetic capacity to irradiance in tree canopies in relation

to leaf nitrogen concentration and leaf mass per unit area. Plant Cell Environ. 25, 343–357.

Moore, B., Braswell, B.H., 1994. Planetary metabolism: understanding the carbon cycle. Ambio 23, 4–12.

Nobre, C.A., Sellers, P.J., Shukla, J., 1991. Amazonian deforestation and regional climate change. J. Climate 4, 957–987.

Parton, W.J., Scurlock, J.M.O., Ojima, D.S., Gilmanov, T.G., Scholes, R.J., Schimel, D.S., Kirchner, T., Menaut, J.-C., Seastedt, T., Garcia-Moya, E., Apinan Kamnalrut, Kinyamario, J.I., 1993. Observations and modeling of biomass and soil organic matter dynamics for the grassland biome worldwide. Global Biogeochem. Cycl. 7, 785–809.

Pearman, I., Thomas, S.M., Thorne, G.N., 1979. Effect of nitrogen fertilizer on photosynthesis of several varieties of winter wheat. Ann. Botany 43, 613–621.

Pielke, R.A., Avissar, R., Raupach, M., Dolman, A.J., Zeng, X., Denning, A.S., 1998. Interactions between the atmosphere and terrestrial ecosystems: influence on weather and climate. Global Change Biol. 4, 461–475.

Pielke, R.A., Cotton, W.R., Walko, R.L., Tremback, C.J., Lyons, W.A., Grasso, L.D., Nicholls, M.E., Moran, M.D., Wesley, D.A., Lee, T.J., Copeland, J.H., 1992. A comprehensive meteorological modeling system—RAMS. Meteorol. Atmos. Phys. 49, 69–91.

Pielke, R.A., Vidale, P.L., 1995. The boreal forest and the polar front. J. Geophys. Res. 100, 25755–25758.

Polcher, J., Laval, K., 1994. The impact of African and Amazonian deforestation on tropical climate. J. Hydrol. 155, 389–405.

Raich, J.W., Nadelhoffer, K., 1989. Belowground carbon allocation in forest ecosystems: global trends. Ecology 70, 1346–1354.

Raich, J.W., Rastetter, E.B., Melillo, J.M., Kicklighter, D.W., Steudler, P.A., Peterson, B.J., Grace, A.L., Moore, B., Vörösmarty, C.J., 1991. Potential net primary productivity in South America: application of a global model. Ecol. Applic. 1, 399–429.

Randall, D.A., Dazlich, D.A., Zhang, C., Denning, A.S., Sellers, P.J., Tucker, C.J., Bounoua, L., Berry, J.A., Collatz, G.J., Field, C.B., Los, S.O., Justice, C.O., Fung, I., 1996. A revised land surface parameterization (SiB2) for atmospheric GCMs. Part III. The greening of the Colorado State University general circulation model. J. Climate 738–763.

Raupach, M.R., 1991. Vegetation–atmosphere interaction in homogeneous and heterogeneous terrain—some implications of mixed-layer dynamics. Vegetation 91, 105–120.

Reichstein, M., Rey, A., Freibauer, A., Tenhunen, J.D., Valentini, R., Banza, J., Casals, P., Cheng, Y., Rosenzweig, J.M., Irvine, J., Joffre, R., Law, B.E., Loustau, D., Miglietta, F., Oechel, W., Ourcival, J.-M., Pereira, J.S., Peressotti, A., Ponti, F., Qi, J., Rambal, S., Rayment, M., Romanya, J., Rossi, F., Tedeschi, V., Tirone, G., Xu, M., Yakir, D., 2003. Modeling temporal and large-scale spatial variability of soil respiration from soil water availability, temperature and vegetation productivity indices. Global Biogeochem. Cycl. 17, 1104.

Riebsame, W.E., 1990. The United States Great Plains. In: Turner, B.L., et al. (Eds.), The Earth as Transformed by Human Action. Cambridge University Press, Cambridge, pp. 561–576.

Schimel, D.S., 1995. Terrestrial ecosystems and the carbon cycle. Global Change Biol. 1, 77–91.

Schlesinger, W., Andrews, J., 2000. Soil respiration and the global carbon cycle. Biogeochemistry 48, 7–20.

Sellers, P.J., Berry, J.A., Collatz, G.J., Field, C.B., Hall, F.G., 1992. Canopy reflectance, photosynthesis, and transpiration. III. A reanalysis using improved leaf models and a new canopy integration scheme. Remote Sens. Environ. 42, 187–216.

Sellers, P.J., Bounoua, L., Collatz, G.J., Randall, D.A., Dazlich, D.A., Los, S.O., Berry, J.A., Fung, I., Tucker, C.J., Field, C.B., Jensen, T.G., 1996a. Comparison of radiative and physiological effects of doubled atmospheric CO_2 on climate. Science 217, 1402–1406.

Sellers, P.J., Los, S.O., Tucker, C.J., Justice, C.O., Dazlich, D.A., Collatz, G.J., Randall, D.A., 1996b. A revised land surface parameterization (SiB2) for atmospheric GCMs. Part II. The generation of global fields of terrestrial parameters from satellite data. J. Climate 9, 706–737.

Sellers, P.J., Randall, D.A., Collatz, G.J., Berry, J.A., Field, C.B., Dazlich, D.A., Zhang, C., Collelo, G.D., Bounoua, L., 1996c. A revised land surface parameterization (SiB2) for atmospheric GCMs. Part I. Model formulation. J. Climate 9, 676–705.

Stohlgren, T.J., Chase, T.N., Pielke, R.A., Kittel, T.G.F., Baron, J.S., 1998. Evidence that local land use practices influence regional climate, vegetation, and stream flow patterns in adjacent natural areas. Global Change Biol. 4, 495–504.

Suyker, A.E., Verma, S.B., 2001. Year-round observations of the net ecosystem exchange of carbon dioxide in a native tallgrass prairie. Global Change Biol. 7, 279–289.

Suyker, A.E., Verma, S.B., Burba, G.G., 2003. Inter-annual variability in net CO_2 exchange in a native tallgrass prairie. Global Change Biol. 9, 255–265.

Taylor, C.M., Harding, R.J., Thorpe, A.J., Bessemoulin, P., 1997. A mesoscale simulation of land surface heterogeneity from HAPEX-Sahel. J. Hydrol. 188–189, 1040–1066.

Turner, B.L., Clark, W.C., Kates, R.W., Richards, J.F., Mathews, J.T., Meyer, W.B., 1990. The Earth as Transformed by Human Action. Cambridge University Press, Cambridge.

VEMAP-Members, 1995. Vegetation/ecosystem modeling and analysis project: comparing biogeography and biogeochemistry models in a continental-scale study of terrestrial ecosystem responses to climate change and CO_2 doubling. Global Biogeochem. Cycl. 9, 407–437.

Wang, G.L., Eltahir, E.A.B., 2000. Role of vegetation dynamics in enhancing the low-frequency variability of the Sahel rainfall. Water Resour. Res. 36, 1013–1021.

Wigmosta, M.S., Leung, L.R., Rykiel, E.J., 1995. Regional modelling of climate-terrestrial ecosystem interactions. J. Biogeography 22, 453–465.

Yan, H., Anthes, R.A., 1988. The effect of variations in surface soil moisture on mesoscale circulations. Monthly Weather Rev. 116, 192–208.

Zeng, N., Neelin, J.D., Lau, K.M., Tucker, C.J., 1999. Enhancement of interdecadal climate variability in the Sahel by vegetation interaction. Science 286, 1537–1540.